Available online at www.sciencedirect.com
ScienceDirect
International Journal of Heat and Mass Transfer 51 (2008) 4496–4505
International Journal of HEAT and MASS TRANSFER
www.elsevier.com/locate/ijhmt

Finite element analysis of natural convection flow in a isosceles triangular enclosure due to uniform and non-uniform heating at the side walls

Tanmay Basak [a], S. Roy [b], S. Krishna Babu [b], A.R. Balakrishnan [a,*]

[a] Department of Chemical Engineering, Indian Institute of Technology Madras, Chennai 600036, India
[b] Department of Mathematics, Indian Institute of Technology Madras, Chennai 600036, India

Received 16 March 2007; received in revised form 10 December 2007
Available online 10 March 2008

Abstract

A penalty finite element analysis with bi-quadratic elements is carried out to investigate the effects of uniform and non-uniform heating of inclined walls on natural convection flows within a isosceles triangular enclosure. Two cases of thermal boundary conditions are considered; case I: two inclined walls are uniformly heated while the bottom wall is cold isothermal and case II: two inclined walls are non-uniformly heated while the bottom wall is cold isothermal. The numerical solution of the problem is presented for various Rayleigh numbers (Ra), ($10^3 \leqslant Ra \leqslant 10^6$) and Prandtl numbers ($Pr$), ($0.026 \leqslant Pr \leqslant 1000$). It has been found that at small Prandtl numbers, geometry does not have much influence on flow structure while at $Pr = 1000$, the stream function contours are nearly triangular showing that geometry has considerable effect on the flow pattern. In addition, the presence of multiple circulations are observed for small Pr ($Pr = 0.026$) which causes wavy distribution of local Nusselt number. It is observed that non-uniform heating produces greater heat transfer rates at the center of the walls than the uniform heating; however, average Nusselt numbers show overall lower heat transfer rates for the non-uniform heating case. Critical Rayleigh numbers for conduction dominant heat transfer cases have been obtained and for convection dominant regimes, power law correlations between average Nusselt number and Rayleigh numbers are presented for specific Prandtl numbers.

Keywords: Penalty finite element method; Natural convection; Triangular enclosure; Non-uniform heating

1. Introduction

Natural convection in a enclosed cavity is important in many engineering applications and in particular, triangular enclosure has received a considerable attention because of its applicability in various fields such as

- Energy related applications, for example: thermal insulation of buildings using air gaps, solar energy collectors, furnaces and fire control in building etc. [1].
- Geophysical applications, for example: differential heating and cooling in lakes, pollutants diffusion in sea and natural convection in reservoir sidearms etc. [2].

Among the earlier reported studies for triangular enclosures, Karyakin et al. [3] and Holtzman et al. [4] described laminar natural convection in isosceles triangular enclosures heated from below and symmetrically cooled from above. Buoyancy driven flows are complex because of essential coupling between the transport properties of the flow and thermal fields. A literature survey shows that a comprehensive review of these problems is well documented in a recent book by Bejan [5]. Further, Del Campo et al. [6] modeled natural convection in triangular

* Corresponding author. Tel.: +91 44 2257 4154; fax: +91 44 2257 0509.
E-mail addresses: tanmay@iitm.ac.in (T. Basak), sjroy@iitm.ac.in (S. Roy), arbala@iitm.ac.in (A.R. Balakrishnan).

0017-9310/$ - see front matter © 2008 Published by Elsevier Ltd.
doi:10.1016/j.ijheatmasstransfer.2007.12.018

Nomenclature

g	acceleration due to gravity, m s^{-2}
J	Jacobian of residual equations
k	thermal conductivity, W m^{-1} K^{-1}
L	height of the triangular cavity, m
N	total number of nodes
Nu	local Nusselt number
p	pressure, Pa
P	dimensionless pressure
Pr	Prandtl number
R	residual of weak form
Ra	Rayleigh number
T	temperature, K
T_h	temperature of hot bottom wall, K
T_c	temperature of cold vertical wall, K
u, v	x and y components of dimensional velocities, respectively
U, V	x and y components of dimensionless velocities, respectively
X, Y	dimensionless distances along x and y coordinates, respectively

Greek symbols

α	thermal diffusivity, m^2 s^{-1}
β	volume expansion coefficient, K^{-1}
γ	penalty parameter
ξ, η	horizontal and vertical coordinates in a unit square, respectively
θ	dimensionless temperature
ν	kinematic viscosity, m^2 s^{-1}
ρ	density, kg m^{-3}
Φ	basis functions
ψ	stream function

Subscripts

b	bottom wall
i	residual number
k	node number
l	left wall
r	right wall

Superscript

n	Newton iterative index

enclosures using Galerkin finite element method with a stream function – vorticity formulation of steady state equations of motion for $A = 0.2$–20 (where A is the aspect ratio) and $Gr = 10^3$–10^6. Their investigation is based on a symmetric boundary condition for a system with heating from below. The solutions obtained were symmetric about midplane. Poulikakos and Bejan [7] investigated the fluid dynamics inside a triangular enclosure with cold upper wall and horizontal bottom wall. They applied the asymptotic methods of Cormack et al. [8] to find approximate steady state regime and temperature distributions inside a triangle when aspect ratio of the enclosure is vanishingly small. This led to the criteria for the existence of distinct thermal and viscous layers along both the walls in steady state. This physical complexity in confined convection is not only a topic for analysis but has equal significance for numerical and experimental investigations. The extensive research based on various numerical simulations reported by Patterson and Imberger [9], Nicolette et al. [10], Hyun and Lee [11], Fusegi et al. [12] establish that several attempts have been made to acquire a basic understanding of natural convection flows and heat transfer characteristics in an enclosure.

The aim of the present paper is to study the circulations and temperature distributions within the triangular enclosure and heat transfer rate at the walls in terms of local and average Nusselt numbers for uniform and non-uniform heating cases. The geometry of the triangular enclosure with boundary conditions is shown in Fig. 1. These boundary conditions resemble summer day boundary conditions where the outside temperature is hot and inside temperature is cold. The jump discontinuities in Dirichlet type of wall boundary conditions at the corner points (see Fig. 1) correspond to computational singularities. In particular, the singularity at the bottom corner nodes needs special attention. One of the ways for handling the problem is assuming the average temperature of the two walls at the corner and keeping the adjacent grid-nodes at the respective wall temperatures similar to the earlier works of square

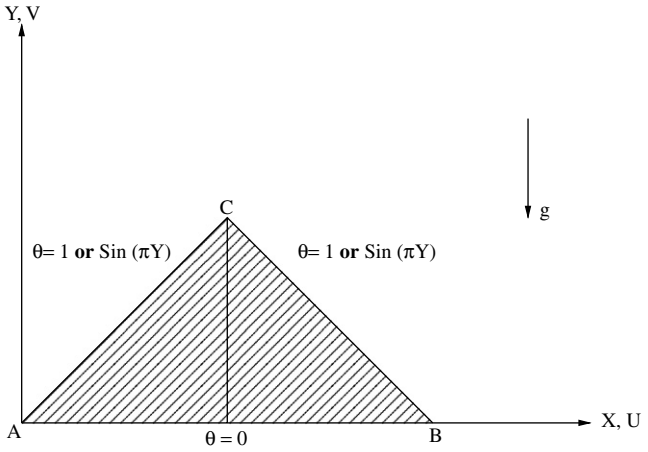

Fig. 1. Schematic diagram of the physical system.

cavity [13,14]. This approach provides the satisfactory results, and the thermal equilibrium of the system is explained in terms of heat transfer rates along the left and right walls. Singularity does not appear in case of sinusoidally heated wall.

In the current study, we have used Galerkin finite element method with penalty parameter to solve the non-linear coupled partial differential equations governing flow and temperature fields for both uniform and sinusoidally varying temperature distribution prescribed at side walls. Non-orthogonal grid generation has been done with iso-parametric mapping [15,16]. The complete explanation about grid generation using iso-parametric mapping is given in Appendix A. Numerical results are obtained to display the circulations and temperature distributions within the triangle and the heat transfer rate for both the walls in terms of local and average Nusselt numbers.

2. Governing equations

The fluid properties are assumed to be constant except the density variation which was determined according to the Boussinesq approximation which is commonly used in buoyancy driven flow. The essence of Boussinesq approximation is that the difference in inertia is neglected but gravity is sufficiently strong to make the specific weight appreciably different between the two liquids of different temperatures. The dimensionless form of the governing equations for steady natural convection flow using conservation of mass, momentum and energy can be obtained with the following variables:

$$X=\frac{x}{L},\quad Y=\frac{y}{L},\quad U=\frac{uL}{\alpha},\quad V=\frac{vL}{\alpha},\quad \theta=\frac{T-T_c}{T_h-T_c},$$
$$P=\frac{pL^2}{\rho\alpha^2},\quad Pr=\frac{\nu}{\alpha},\quad Ra=\frac{g\beta(T_h-T_c)L^3Pr}{\nu^2}, \tag{1}$$

and the governing equations are:

$$\frac{\partial U}{\partial X}+\frac{\partial V}{\partial Y}=0, \tag{2}$$
$$U\frac{\partial U}{\partial X}+V\frac{\partial U}{\partial Y}=-\frac{\partial P}{\partial X}+Pr\left(\frac{\partial^2 U}{\partial X^2}+\frac{\partial^2 U}{\partial Y^2}\right), \tag{3}$$
$$U\frac{\partial V}{\partial X}+V\frac{\partial V}{\partial Y}=-\frac{\partial P}{\partial Y}+Pr\left(\frac{\partial^2 V}{\partial X^2}+\frac{\partial^2 V}{\partial Y^2}\right)+RaPr\theta, \tag{4}$$
$$U\frac{\partial \theta}{\partial X}+V\frac{\partial \theta}{\partial Y}=\frac{\partial^2 \theta}{\partial X^2}+\frac{\partial^2 \theta}{\partial Y^2}, \tag{5}$$

with the boundary conditions (see Fig. 1)

$$\begin{aligned}
&U(X,0)=0=V(X,0),\quad \theta(X,0)=0 \text{ on AB},\quad \forall 0\leqslant X\leqslant 2,\\
&U(X,Y)=0=V(X,Y),\quad \theta(X,Y)=1 \text{ or}\\
&\quad \sin(\pi Y) \text{ on AC},\quad Y=X,\forall 0\leqslant X\leqslant 1,\\
&U(X,Y)=0=V(X,Y),\quad \theta(X,Y)=1 \text{ or}\\
&\quad \sin(\pi Y) \text{ on BC},\quad Y=2-X,\forall 1\leqslant X\leqslant 2.
\end{aligned} \tag{6}$$

3. Solution procedure and post-processing

The momentum and energy balance equations (Eqs. (3)–(5)) are solved using the Galerkin finite element method. The continuity equation (2) is used as a constraint due to mass conservation and this constraint may be used to obtain the pressure distribution. In order to solve Eqs. (3)–(5), the penalty finite element method is used where the pressure P is eliminated by a penalty parameter γ and the incompressibility criteria given by Eq. (2) results in

$$P=-\gamma\left(\frac{\partial U}{\partial X}+\frac{\partial V}{\partial Y}\right). \tag{7}$$

The continuity equation (2) is automatically satisfied for large values of γ. Typical value of γ that yields consistent solutions is 10^7. Using Eq. (7), the momentum balance Eqs. (3) and (4) reduce to

$$U\frac{\partial U}{\partial X}+V\frac{\partial U}{\partial Y}=\gamma\frac{\partial}{\partial X}\left(\frac{\partial U}{\partial X}+\frac{\partial V}{\partial Y}\right)+Pr\left(\frac{\partial^2 U}{\partial X^2}+\frac{\partial^2 U}{\partial Y^2}\right), \tag{8}$$
$$U\frac{\partial V}{\partial X}+V\frac{\partial V}{\partial Y}=\gamma\frac{\partial}{\partial Y}\left(\frac{\partial U}{\partial X}+\frac{\partial V}{\partial Y}\right)+Pr\left(\frac{\partial^2 V}{\partial X^2}+\frac{\partial^2 V}{\partial Y^2}\right)+RaPr\theta. \tag{9}$$

The system of equations (5), (8) and (9) with boundary conditions is solved by using Galerkin finite element method [15]. Since the solution procedure is explained in an earlier work [14], the detailed description is not included in this paper. The numerical solutions are obtained in terms of the velocity components (U,V) and stream function (ψ) is evaluated using the relationship between the stream function (ψ) and the velocity components [17], where the stream function (ψ) is defined in the usual way as $U=\frac{\partial\psi}{\partial Y}$ and $V=-\frac{\partial\psi}{\partial X}$. It may be noted that, the positive sign of ψ denotes anti-clockwise circulation and the clockwise circulation is represented by the negative sign of ψ. The no-slip condition is valid at all boundaries as there is no cross flow, hence $\psi=0$ is used for the boundaries.

The heat transfer coefficient in terms of the local Nusselt number (Nu) is defined by

$$Nu=-\frac{\partial\theta}{\partial n}, \tag{10}$$

where n denotes the normal direction on a plane. The local Nusselt numbers at bottom wall (Nu_b), left wall (Nu_l) and right wall (Nu_r) are defined as

$$Nu_b=-\sum_{i=1}^{9}\theta_i\frac{\partial\Phi_i}{\partial Y}, \tag{11}$$
$$Nu_l=\sum_{i=1}^{9}\theta_i\left(-\frac{1}{\sqrt{2}}\frac{\partial\Phi_i}{\partial X}+\frac{1}{\sqrt{2}}\frac{\partial\Phi_i}{\partial Y}\right) \tag{12}$$

and

$$Nu_r=\sum_{i=1}^{9}\theta_i\left(\frac{1}{\sqrt{2}}\frac{\partial\Phi_i}{\partial X}+\frac{1}{\sqrt{2}}\frac{\partial\Phi_i}{\partial Y}\right). \tag{13}$$

The average Nusselt numbers at the bottom and side walls are

$$\overline{Nu_b} = \frac{\int_0^2 Nu_b dX}{X|_0^2} = \frac{1}{2}\int_0^2 Nu_b dX \tag{14}$$

and

$$\overline{Nu_l} = \overline{Nu_r} = \frac{1}{\sqrt{2}}\int_0^{\sqrt{2}} Nu_l dS. \tag{15}$$

Here dS denotes the elemental length along the side walls of the triangle as seen in Fig. 1.

4. Results and discussion

4.1. Numerical tests

The computational domain in $\xi - \eta$ coordinates (see Appendix A) consists of 20×20 bi-quadratic elements which correspond to 41×41 grid points. It may be noted that the computational grid in the triangular domain is generated via mapping the triangular domain into a square domain in $\xi - \eta$ coordinate system as shown in Fig. 2 and the procedure is outlined in Appendix A. The bi-quadratic elements with lesser number of nodes smoothly capture the non-linear variations of the field variables which are in contrast with finite difference/finite volume solutions available in the literature [18,19].

In the current investigation, Gaussian quadrature based finite element method provides the smooth solutions at the interior domain including the corner regions as evaluation of residuals depends on interior Gauss points and thus the effect of corner nodes are less pronounced in the final solution. In general, the Nusselt numbers for finite difference/finite volume based methods are calculated at any surface using some interpolation functions which are now avoided in the current work. The present finite element approach offers special advantage on evaluation of local Nusselt number at the left, right and bottom walls as the element basis functions are used to evaluate the heat flux [13]. For the two cases (Cases I and II) considered here, the Rayleigh number is varied from 10^3 to 10^6 for a fixed Prandtl number, while the plots are obtained for $Pr = 0.026$–1000. Local and average Nusselt numbers are evaluated for all the cases. The comparative study was made for uniform and non-uniform heating of the side walls. The detailed analysis has been shown in various sections as follows. For brevity, only the most important results are presented in the following sections.

4.2. Uniform heating of side walls (case I)

Figs. 3–8 illustrate the stream function and isotherm contours when the side walls are uniformly heated while the bottom wall is maintained at constant cold tempera-

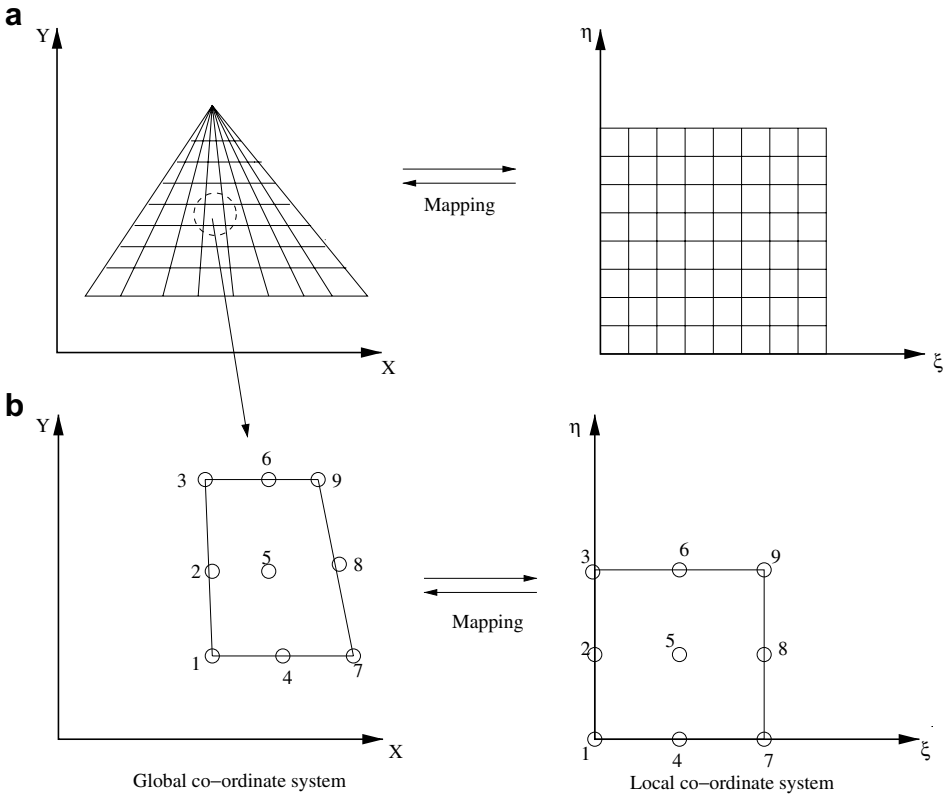

Fig. 2. (a) The mapping of triangular domain to a square domain in $\xi - \eta$ coordinate system and (b) the mapping of an individual element to a single element in $\xi - \eta$ coordinate system.

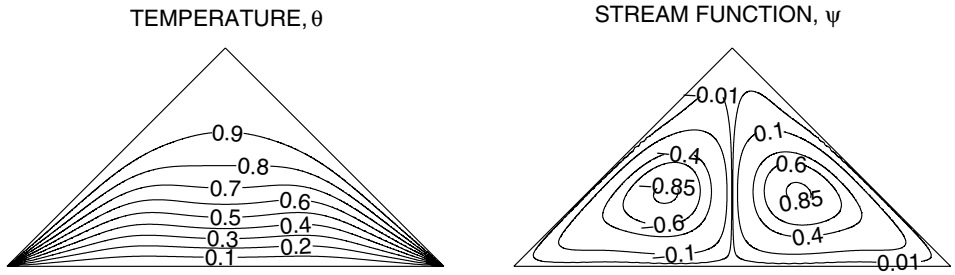

Fig. 3. Temperature and stream function contours for cold bottom wall, $\theta(X,0)=0$ and uniformly heated inclined walls, $\theta(X,Y)=1$, with $Ra=2\times10^4$ and $Pr=0.026$ (Case I). Clockwise and anti-clockwise flows are shown with negative and positive signs of stream function, respectively.

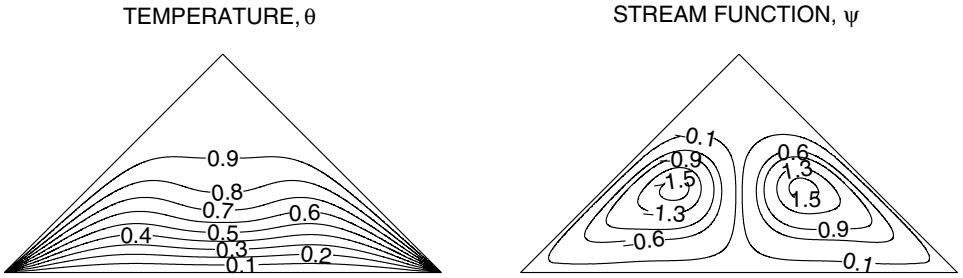

Fig. 4. Temperature and stream function contours for cold bottom wall, $\theta(X,0)=0$ and uniformly heated inclined walls, $\theta(X,Y)=1$, with $Ra=10^5$ and $Pr=0.026$ (Case I). Clockwise and anti-clockwise flows are shown with negative and positive signs of stream function, respectively.

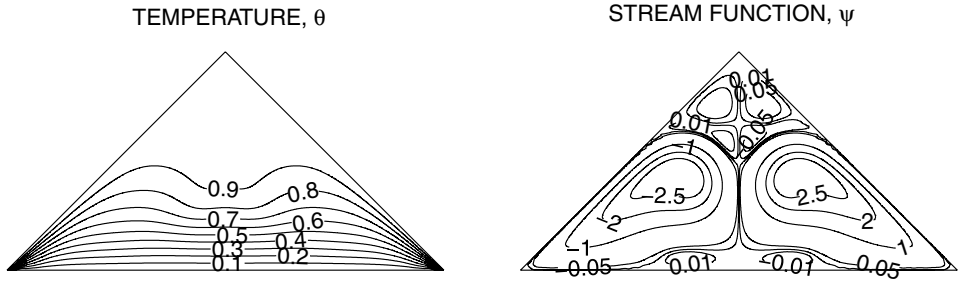

Fig. 5. Temperature and stream function contours for cold bottom wall, $\theta(X,0)=0$ and uniformly heated inclined walls, $\theta(X,Y)=1$, with $Ra=7\times10^5$ and $Pr=0.026$ (Case I). Clockwise and anti-clockwise flows are shown with negative and positive signs of stream function, respectively.

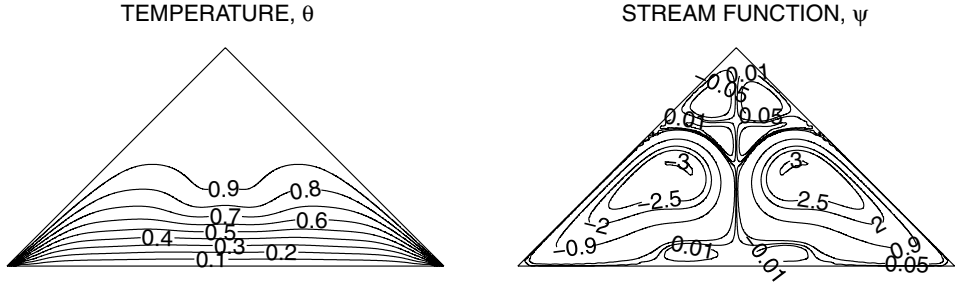

Fig. 6. Temperature and stream function contours for cold bottom wall, $\theta(X,0)=0$ and uniformly heated inclined walls, $\theta(X,Y)=1$, with $Ra=10^6$ and $Pr=0.026$ (Case I). Clockwise and anti-clockwise flows are shown with negative and positive signs of stream function, respectively.

ture. The fluid near the inclined portion of the enclosures is hotter than the fluid near the cold bottom wall and hence the fluid near the inclined walls have lower density than those near the cold bottom wall. Consequently, the fluid near the hot inclined walls move upward resulting in two oppositely rotating circulations in the enclosure with eye of vortices located at the center of each half of the cross-section. It is observed that, the left half of axis of symmetry gives clock wise circulations whereas right half of axis of symmetry gives anti-clockwise circulation pattern. At low

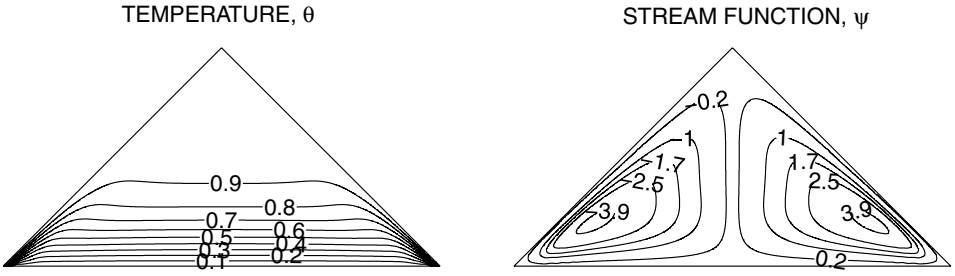

Fig. 7. Temperature and stream function contours for cold bottom wall, $\theta(X,0) = 0$ and uniformly heated inclined walls, $\theta(X,Y) = 1$, with $Ra = 10^6$ and $Pr = 0.7$ (Case I). Clockwise and anti-clockwise flows are shown with negative and positive signs of stream function, respectively.

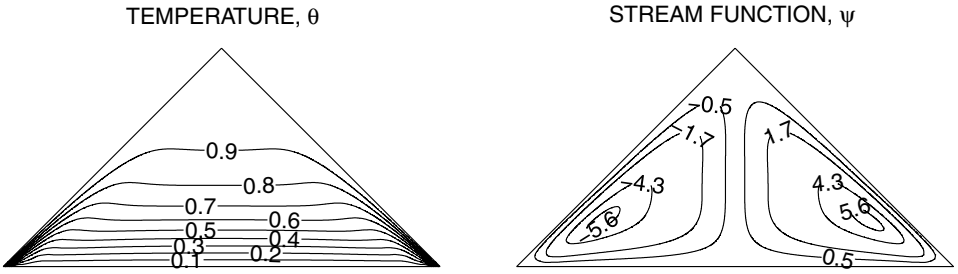

Fig. 8. Temperature and stream function contours for cold bottom wall, $\theta(X,0) = 0$ and uniformly heated inclined walls, $\theta(X,Y) = 1$, with $Ra = 10^6$ and $Pr = 1000$ (Case I). Clockwise and anti-clockwise flows are shown with negative and positive signs of stream function, respectively.

Rayleigh number, the isotherm lines are smooth and monotonic and the magnitudes of the stream function contours are quite small. This illustrates that at small Ra, the heat transfer is mostly due to conduction. The temperature contours are smooth curves which span the entire enclosure and they are generally symmetric with respect to vertical center line. At $Ra = 2 \times 10^4$ and $Pr = 0.026$, the temperature contours for $\theta \geqslant 0.2$ start getting deformed towards the bottom wall (Fig. 3). The presence of significant convection is also exhibited in the temperature contours which get pushed towards the central portion of the bottom wall. The critical Rayleigh number (for this case: $Ra = 2 \times 10^4$) may be obtained from asymptotes of average Nusselt number vs Rayleigh number plot as discussed later. It may be noted that conduction is dominant below the critical Ra. At $Ra = 10^5$ and $Pr = 0.026$, the buoyancy driven circulation inside the cavity also increases as seen from the greater magnitudes of the stream function (see Fig. 4). The circulations are greater near the center and least at the wall due to no-slip boundary conditions. It is observed that the isotherms are compressed towards the bottom wall as seen in Fig. 4. It may also be noted that the regime near the top corner has no significant thermal gradient resulting in no circulations. As Rayleigh number increases to 7×10^5 for $Pr = 0.026$, isotherms are further compressed towards the bottom wall and therefore the deformation occurs in the stream function near the central symmetric line (see Fig. 5). It is also seen that secondary circulations are developed near to the intersection of the inclined walls. In addition, the temperature contours with $\theta \geqslant 0.7$ start getting deformed near the central regime due to secondary circulations. As Ra further increases to $Ra = 10^6$ for $Pr = 0.026$ (see Fig. 6) the temperature contours with $0.9 \leqslant \theta \leqslant 0.7$ within the domain further condense near the central regime due to stronger secondary circulations.

As Pr increases from 0.026 to 0.7, the secondary circulations are suppressed and due to increase of Pr, the strength of primary circulations is increased as seen in Fig. 7. At $Ra = 10^6$ and $Pr = 0.7$, the circulations near the central regime are stronger and consequently the temperature contours with $\theta \geqslant 0.2$ are found to be compressed towards the bottom wall. Similar situation is also observed for $Pr = 1000$ as seen in Fig. 8. Comparative studies on Figs. 7 and 8 show that, as Pr increases from 0.7 to 1000, the values of stream function and isotherms in the core cavity increase. It may be seen that the greater circulations due to higher Pr lead to elliptical stream function deformed towards the corner portions of bottom wall. At high Pr, the stream functions, except at the central regime are almost triangular indicating higher intensity of flows. Effects of Prandtl number for various Rayleigh numbers on local and average Nusselt number are discussed later in detail.

4.3. Non-uniform heating of side walls (case II)

Figs. 9–11 illustrate the stream function and isotherm contours when the inclined walls are non-uniformly heated via sinusoidal functions. As seen in Figs. 3–8, uniform heating of inclined walls causes a finite discontinuity in Dirichlet type of boundary conditions for the temperature distribution at both edges of the bottom wall. In contrast,

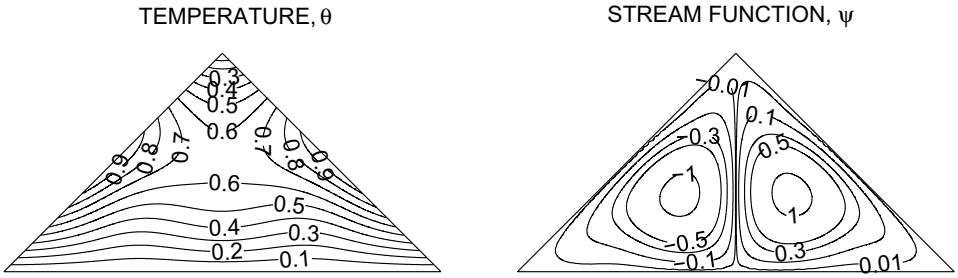

Fig. 9. Temperature and stream function contours for cooled bottom wall, $\theta(X,0)=0$ and non-uniformly heated inclined walls, $\theta(X,Y)=\sin(\pi Y)$, with $Ra=2\times10^4$ and $Pr=0.026$ (Case II). Clockwise and anti-clockwise flows are shown with negative and positive signs of stream function, respectively.

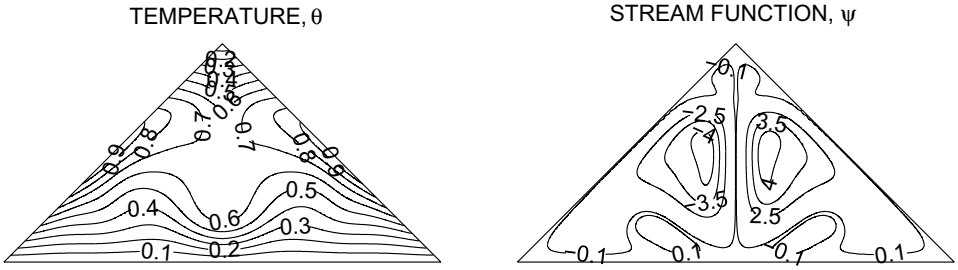

Fig. 10. Temperature and stream function contours for cooled bottom wall, $\theta(X,0)=0$ and non-uniformly heated inclined walls, $\theta(X,Y)=\sin(\pi Y)$, with $Ra=10^6$ and $Pr=0.026$ (Case II). Clockwise and anti-clockwise flows are shown with negative and positive signs of stream function, respectively.

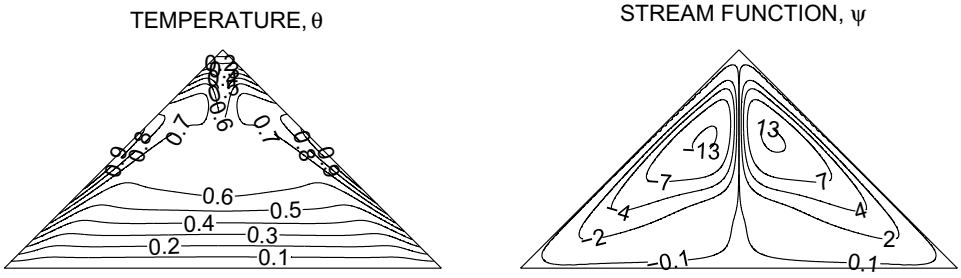

Fig. 11. Temperature and stream function contours for cooled bottom wall, $\theta(X,0)=0$ and non-uniformly heated inclined walls, $\theta(X,Y)=\sin(\pi Y)$, with $Ra=10^6$ and $Pr=1000$ (Case II). Clockwise and anti-clockwise flows are shown with negative and positive signs of stream function, respectively.

the non-uniform heating removes the singularity at the edges of bottom wall and provides a smooth temperature distribution in the entire enclosure. Simulations indicate that the isotherms are almost smooth and parallel and magnitude of stream function is very low at smaller Ra (figure not shown). Similar situations are also observed for uniform heating case. It may be noted that the conduction dominant heat transfer is observed upto $Ra=2\times10^4$. At $Ra=2\times10^4$, the isotherms with $\theta\leqslant0.5$ start getting pushed towards the bottom wall (see Fig. 9). It is interesting to observe that the top portion of the side wall within the cavity have significant thermal gradient and that results in stronger circulations compared to the uniform heating case. At $Ra=10^6$ and $Pr=0.026$, the isotherms with $\theta\leqslant0.6$ are pushed further towards the bottom wall and consequently the temperature gradients near the bottom wall are significant. This is due to the fact that the strong primary circulations occur near the bottom wall (Fig. 10). In addition, the secondary circulations also occur near the center of the bottom wall. This further pushes the temperature contours near the center of the bottom wall. As Pr increases further to $Pr=1000$ for $Ra=10^6$, it is observed that the greater circulations pushes the isotherms towards the side walls and bottom wall as seen in Fig. 11. In addition, the greater circulations near the top corner pushes the isotherms within a very narrow region at the vertex and that results in large thermal gradient at the top corner point. In contrast, the intensity of circulations near the bottom corner point is large for uniform heating and large thermal gradient occurs near the bottom wall. Due to non-uniform heating of inclined walls, the heating rate near the bottom corners of the inclined walls is generally lower. Results indicate that the strength of the circulations is more for non-uniform heating case than uniform heating.

4.4. Heat transfer rates: local Nusselt numbers

Fig. 12a and b display the effects of Ra and Pr on the local Nusselt number at the cold bottom wall and hot inclined walls. In case of uniform heating of the bottom wall (see Fig. 12a), due to presence of discontinuity in the temperature boundary condition at the edges of bottom wall, the heat transfer rate is very high at these corners and it reduces towards the middle of the bottom wall as the compression of thermal contours is minimum at the middle for $Ra = 10^3$. The central regime of the bottom wall ($X = 1$) corresponds to large Nu as the compression of the isotherms occurs due to the presence of secondary circulations near the central regime of the bottom wall. At the inclined wall (see Fig. 12b), heat transfer rate is maximum at the bottom edge and minimum at the top edge for all Rayleigh numbers. As Ra increases from 10^3 to 10^5, isotherm lines are pushed towards the bottom wall from the inclined walls due to the presence of secondary circulations. Therefore, at the junction of bottom wall, the thermal gradients are relatively more and therefore the heat transfer rate is maximum at the bottom edge of the inclined wall.

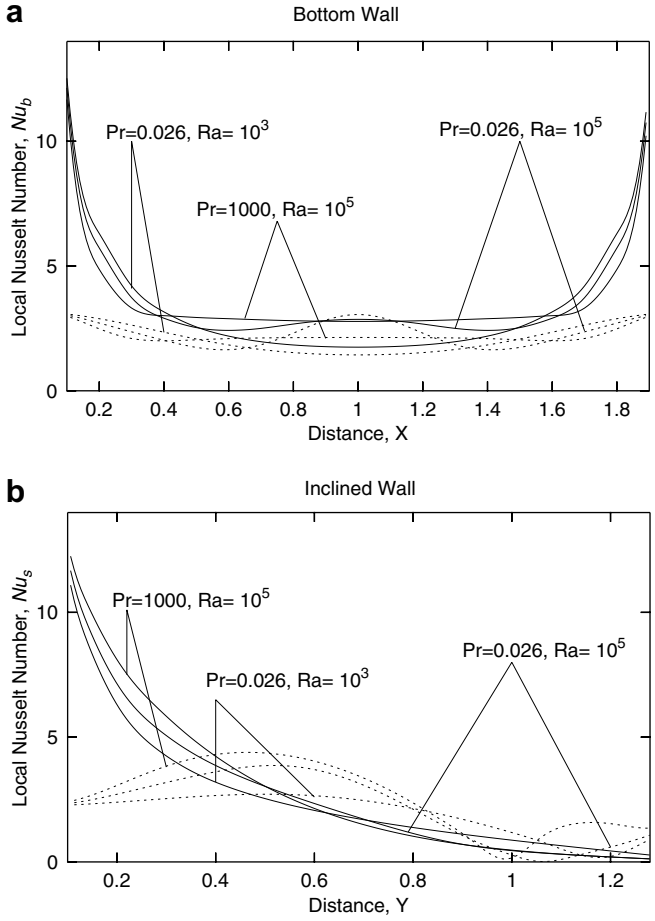

Fig. 12. Variation of local Nusselt number with distance for $Pr = 0.026$ and 1000 at (a) bottom wall (b) inclined wall for uniformly (—) and non-uniformly (- - -) heated inclined walls and cold isothermal bottom wall.

It is seen that the spatial distribution of local Nusselt number for the inclined wall at higher Rayleigh numbers is wavy in nature.

In the case of non-uniform heating (see Fig. 12a), the local Nusselt number is almost constant for $Ra = 10^3$ throughout the bottom wall due to conduction dominant mode of heat transfer. As Ra increases from 10^3 to 10^5, there is a maximum value of thermal gradient at $X = 1$ due to the presence of secondary circulations and that results in maximum local heat transfer rate (Nu) at about $X = 1$. Thus, the non-uniform heating strategy produces a sinusoidal type of local heat transfer rate with its maximum value at the center and edges of bottom wall. At the inclined wall (see Fig. 12b), the local Nusselt number curve for $Ra = 10^3$ shows monotonic decrease from bottom edge to a certain region near to top edge of the inclined wall and local Nu has a maximum value at the top edge of the inclined wall due to the compression of isotherms. Note that, the local Nusselt number have more wavy distributions for smaller Prandtl number ($Pr = 0.026$) as seen in Fig. 12b due to stronger primary and secondary circulations. At $Pr = 1000$, there are two local maxima of local Nusselt number for the inclined wall as the isotherms are compressed near the top corner and the bottom portion of inclined wall.

4.5. Overall heat transfer and average Nusselt numbers

Fig. 13 illustrate the average Nusselt number variations along the bottom and inclined walls for various Rayleigh and Prandtl numbers. As a verification of the thermal equilibrium of the present steady state system, numerical values of the average Nusselt numbers on bottom and inclined walls are compared and it is found that the average Nu of bottom wall is nearly $\sqrt{2}$ times of average Nu (within 1% error) of inclined wall as the length of the inclined wall is $\sqrt{2}$. The current finite element method based analysis is quite robust to establish the thermal equilibrium and the investigations on thermal equilibrium were not reported by earlier works which are based on finite volume or finite difference methods. The critical Rayleigh number is obtained from the semi-log plot of average Nusselt number versus Rayleigh number and at the critical Rayleigh number the transition from conduction dominant mode into convection dominant mode takes place. It is seen that the average Nusselt number increases significantly with Prandtl number in the case of uniform heating. It may be remarked that the overall heat transfer rate (average Nusselt number) is less in non-uniform heating as compared to uniform heating due to less heat input to the system for all Prandtl number regimes. For non-uniform heating case, the increase in average Nusselt number with Rayleigh number is monotonic for small Pr (see Fig. 13). It is also observed that the correlations of average Nusselt numbers and Rayleigh numbers could not be established for $Pr = 1000$, since the variation of average Nusselt number with Rayleigh number is not monotonic.

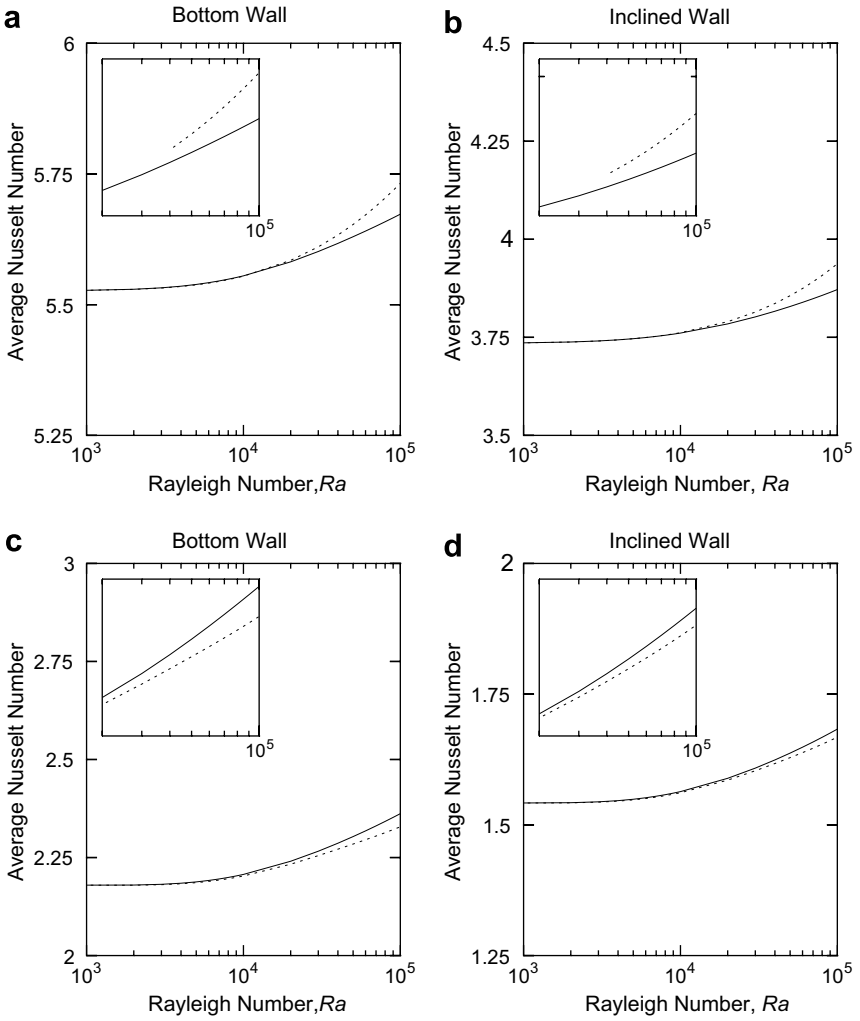

Fig. 13. Variation of average Nusselt number with Rayleigh number for uniformly heated [(a) and (b)] and non-uniformly heated inclined walls [(c) and (d)] with $Pr = 0.026$; (—) and $Pr = 0.7$ (- - -). The insets show the log–log plot of average Nusselt number vs. Rayleigh number for convection dominant regimes.

The insets show the log–log plot for average Nusselt number vs Rayleigh number for convection dominant regimes. The log–log linear plot is obtained with more than 20 data sets. A least square curve is fitted and the overall error is limited within 1%. The following correlations with Prandtl numbers ($Pr = 0.026$ and 0.7) are obtained for case I (uniform heating) and case II (non-uniform heating) as follows:

Case I: Uniform heating of inclined walls

$$\begin{aligned}\overline{Nu}_b &= \sqrt{2}\overline{Nu}_s \\ &= 5.0464Ra^{0.0101}, \quad Ra \geqslant 2.0\times10^4; \quad Pr = 0.026 \\ &= 4.6013Ra^{0.0190}, \quad Ra \geqslant 4.0\times10^4; \quad Pr = 0.7 \end{aligned} \tag{16}$$

Case II: Non-uniform heating of inclined walls

$$\begin{aligned}\overline{Nu}_b &= \sqrt{2}\overline{Nu}_s \\ &= 1.6130Ra^{0.0330}, \quad Ra \geqslant 2.0\times10^4; \quad Pr = 0.026 \\ &= 1.7249Ra^{0.0260}, \quad Ra \geqslant 2.0\times10^4; \quad Pr = 0.7 \end{aligned} \tag{17}$$

5. Conclusions

The prime objective of the current investigation is to analyze the temperature and flow field with detailed analysis on heat transfer evaluation for natural convection in triangular enclosure. The penalty finite element method helps to obtain smooth solutions in terms of stream function and isotherm contours for wide ranges of $Ra(Ra = 10^3 - 10^6)$ and $Pr(Pr = 0.026 - 1000)$ with uniform and non-uniform heating of the side walls. Results indicate that at low Rayleigh number ($Ra = 10^3$), the isotherm lines are smooth and monotonic and heat transfer is primarily due to conduction. It was observed that the conduction heat transfer mode was dominant upto $Ra \leqslant 2\times10^4$ during uniform and non-uniform heating of the side walls with $Pr = 0.026$. At the onset of convection dominant mode, the temperature contour lines get compressed towards central regime of the bottom wall. As Ra increases further for $Pr = 0.026$, the isotherm contours are pushed more towards the bottom wall and the secondary circulations

develop near the intersection of the inclined walls. It has been observed that at lower Prandtl number, the compression of temperature contours is more and secondary circulations are observed. Further results show that, as Pr increases from 0.026 to 1000, the values of stream function and isotherms in the core cavity increase. It is also found that at small Prandtl numbers geometry does not have much influence on flow structure. At high Prandtl numbers geometry has considerable effect, stream function contours are nearly triangular in shape. It is observed that the local Nusselt numbers are maximum at the bottom corner points and due to secondary circulations, the local Nusselt number distribution show wavy nature for high Ra with $Pr = 0.026$ for both uniform and non-uniform heating cases. For non-uniform heating case, the sinusoidal distribution of local Nusselt number at the inclined wall is observed for all Prandtl number regimes. In addition, the lower Prandtl number corresponds to more secondary circulations and flow separations. The average Nusselt number illustrates overall lower heat transfer rates for sinusoidal heating cases. The average Nusselt number is found to follow power law variation with Rayleigh number for convection dominant regimes for Pr ($Pr = 0.026 - 0.7$).

Appendix A

The name iso-parametric derives from the fact that the same parametric function describing the geometry may be used for interpolating spatial variable within an element. Fig. 2 shows a triangular domain with trapezoidal elements with the mapping to a square domain. The transformation between (x, y) and (ξ, η) coordinates can be defined by

$$X = \sum_{k=1}^{9} \Phi_k(\xi, \eta) x_k$$

and

$$Y = \sum_{k=1}^{9} \Phi_k(\xi, \eta) y_k.$$

Here (x_k, y_k) are the X, Y coordinates of the k nodal points as seen in Fig. 2a and b and $\Phi_k(\xi, \eta)$ is the basis function. The nine basis functions are:

$$\Phi_1 = (1 - 3\xi + 2\xi^2)(1 - 3\eta + 2\eta^2)$$
$$\Phi_2 = (1 - 3\xi + 2\xi^2)(4\eta - 4\eta^2)$$
$$\Phi_3 = (1 - 3\xi + 2\xi^2)(-\eta + 2\eta^2)$$
$$\Phi_4 = (-\xi + 2\xi^2)(1 - 3\eta + 2\eta^2)$$
$$\Phi_5 = (-\xi + 2\xi^2)(4\eta - 4\eta^2)$$
$$\Phi_6 = (-\xi + 2\xi^2)(-\eta + 2\eta^2)$$
$$\Phi_7 = (4\xi - 4\xi^2)(1 - 3\eta + 2\eta^2)$$
$$\Phi_8 = (4\xi - 4\xi^2)(4\eta - 4\eta^2)$$
$$\Phi_9 = (4\xi - 4\xi^2)(-\eta + 2\eta^2)$$

The above basis functions are used for mapping the triangular domain or elements within the triangle into square domain and the evaluation of integrals of residuals.

References

[1] K.A. Joudi, I.A. Hussein, A.A. Farhan, Computational model for a prism shaped storage solar collector with a right triangular cross-section, Energy Convers. Manage. 45 (2004) 391–409.

[2] C. Lei, J.C. Patterson, Natural convection in a reservoir sidearm subject to solar radiation: experimental observations, Exp. Fluid 32 (2002) 590–599.

[3] Yu.E. Karyakin, Yu.A. Sokovishin, O.G. Martynenko, Transient natural convection in triangular enclosures, Int. J. Heat Mass Transfer 31 (1988) 1759–1766.

[4] G.A. Holtzman, R.W. Hill, K.S. Ball, Laminar natural convection in isosceles triangular enclosures heated from below and symmetrically cooled from above, J. Heat Transfer 122 (2000) 485–491.

[5] A. Bejan, Convection Heat Transfer, third ed., Wiley, Hoboken, NJU, 2004.

[6] E.M. Del Campo, M. Sen, E. Ramos, Analysis of laminar natural convection in a triangular enclosure, Numer. Heat Transfer 13 (1988) 353–372.

[7] D. Poulikakos, A. Bejan, The fluid dynamics of an attic space, J. Fluid Mech. 131 (1983) 251–269.

[8] D.E. Cormack, L.G. Leal, J. Imberger, Natural convection in a shallow cavity with differentially heated end walls. Part 1. Asymptotic theory, J. Fluid Mech. 65 (1974) 209–229.

[9] J. Patterson, J. Imberger, Unsteady natural convection in a rectangular cavity, J. Fluid Mech. 100 (1980) 65–86.

[10] V.F. Nicolette, K.T. Yang, J.R. Lloyd, Transient cooling by natural convection in a two dimensional enclosure, Int. J. Heat Mass Transfer 28 (1985) 1721–1732.

[11] J.M. Hyun, J.W. Lee, Numerical solutions of transient natural convection in a square cavity with different sidewall temperatures, Int. J. Heat Fluid Flow 10 (1989) 146–151.

[12] T. Fusegi, J.M. Hyun, K. Kuwahara, Natural convection in a differentially heated square cavity with internal heat generation, Numer. Heat Transfer A 21 (1992) 215–229.

[13] S. Roy, T. Basak, Finite element analysis of natural convection flows in a square cavity with non-uniformly heated wall(s), Int. J. Eng. Sci. 43 (2005) 668–680.

[14] T. Basak, S. Roy, A.R. Balakrishnan, Effects of thermal boundary conditions on natural convection flows within a square cavity, Int. J. Heat Mass Transfer 49 (2006) 4525–4535.

[15] J.N. Reddy, An Introduction to the Finite Element Method, McGraw-Hill, NY, 1993.

[16] T.J. Chung, Computational Fluid Dynamics, Cambridge University Press, London, 2002.

[17] G.K. Batchelor, An Introduction to Fluid Dynamics, Cambridge University Press, 1993.

[18] H. Asan, L. Namli, Numerical simulation of buoyant flow in a roof of triangular cross section under winter day boundary conditions, Energy Buildings 33 (2001) 753–757.

[19] R. Jyotsna, S.P. Vanka, Multigrid calculation of steady, viscous-flow in a triangular cavity, J. Comput. Phys. 122 (1995) 107–117.